

System stabilization with policy optimization on unstable latent manifolds

Steffen W. R. Werner* Benjamin Peherstorfer†

**Department of Mathematics and Division of Computational Modeling and Data Analytics,
Academy of Data Science, Virginia Tech, Blacksburg, VA 24061, USA.*

Email: steffen.werner@vt.edu, ORCID: [0000-0003-1667-4862](https://orcid.org/0000-0003-1667-4862)

†Courant Institute of Mathematical Sciences, New York University, New York, NY 10012, USA.

Email: pehersto@cims.nyu.edu, ORCID: [0000-0002-1558-6775](https://orcid.org/0000-0002-1558-6775)

Abstract: Stability is a basic requirement when studying the behavior of dynamical systems. However, stabilizing dynamical systems via reinforcement learning is challenging because only little data can be collected over short time horizons before instabilities are triggered and data become meaningless. This work introduces a reinforcement learning approach that is formulated over latent manifolds of unstable dynamics so that stabilizing policies can be trained from few data samples. The unstable manifolds are minimal in the sense that they contain the lowest dimensional dynamics that are necessary for learning policies that guarantee stabilization. This is in stark contrast to generic latent manifolds that aim to approximate all—stable and unstable—system dynamics and thus are higher dimensional and often require higher amounts of data. Experiments demonstrate that the proposed approach stabilizes even complex physical systems from few data samples for which other methods that operate either directly in the system state space or on generic latent manifolds fail.

Keywords: nonlinear systems, feedback stabilization, context-aware learning, neural networks, reinforcement learning

Mathematics subject classification: 37N35, 68T07, 90C30, 93C57, 93D15

1 Introduction

Dynamical systems are core building blocks for describing the time-dependent behavior of phenomena of interest in science and engineering, including physical relationships [11], engineering systems [28] as well as agents acting in environments in social sciences [62]. A major task is controlling dynamical systems so that they are steered towards desired states. In this work, we consider the specific control task of stabilizing dynamical systems, which means that states have to remain in the same neighborhood of the desired system behavior despite small perturbations [38, 46]. Stability is an important property because reasonable actions in dynamic environments should avoid that the system leaves the desired behavior. In many cases, stability is even a prerequisite for meaningful predictions about how the system states evolve in the future. One approach for stabilizing systems is via feedback

control, which means that external inputs are constructed based on the current state of the system such that the future system states remain within the neighborhood of the desired steady state (equilibrium point).

Classical control techniques rely on the governing equations of the dynamics [13]. In contrast, data-driven control methods [13, 17, 74] and reinforcement learning [64] learn control policies from data. Despite immense progress on reinforcement learning and related machine learning methods for control, stabilizing systems from data remains challenging. First, recall that the aim is to stabilize dynamical systems and thus it is reasonable to expect that the open-loop systems without stabilizing policies are unstable. Therefore, systems can be queried only for short time horizons before instabilities are triggered, which makes collecting state trajectories that are informative about the system challenging. In fact, intermediate policies during the learning process often lead to additional destabilization, which makes data collection even more challenging. Second, the dimension of the parametrization, e.g., the number of weights and biases of a deep-network parametrization of a policy in reinforcement learning, typically grows with the complexity of the dynamics described by the system. In particular, the number of parameters grows with the state dimension and the number of control inputs. This means that the optimization space, over which a policy is trained, can be rich and thus large amounts of data are typically required to find informative search directions, which starkly conflicts with the challenge mentioned above that collecting data samples of unstable systems can be problematic [14, 53]. Third, simulating or querying systems can be expensive. Either because numerical simulations have to be performed or because physical experiments need to be conducted. In any case, each query to collect a data point is expensive and thus typically only few data points can be collected. There are many methods for learning surrogate models from data, e.g., dynamic mode decomposition [12, 35, 41, 54, 57, 66, 73], operator inference [31, 49, 50, 52, 55, 61], sparse identification methods [14, 56], the Loewner framework [3, 16, 23, 40, 58, 59], and others [9, 27, 67]; however, having only few data points also means that training such data-driven surrogate models is challenging and often intractable.

In this work, we propose to first learn a low-dimensional manifold on which exactly those dynamics of the system evolve that are important for stabilization, and then to learn a policy for stabilizing the dynamics on that manifold only; see Figure 1 for a comparison between our proposed method and traditional reinforcement learning. The key insight is that the latent manifolds that are typically used for finding low-dimensional models in model reduction, e.g., via training autoencoders [5, 26, 29] on state trajectories, quadratic manifolds [6, 19, 60], or even just computing the principal components [7], are poorly suited for stabilization. Instead, we restrict the system to the manifold of unstable dynamics [33, 71] that captures exactly those dynamics that are relevant for the task of stabilization. Because of the low dimensionality of the unstable manifold in many applications of interest—see [71] and Figure 2—we can use low-dimensional parametrizations such as deep networks with few parameters for the policies, which reduce the amount of computational resources needed for the training process. Additionally, the learning on unstable manifolds can be combined with multi-fidelity concepts [51] to first pre-train a policy on a cheap-to-evaluate approximation of the unstable dynamics before the policy is fine-tuned and certified on the actual system of interest; see [70] for a multi-fidelity optimization approach for robust control. The multi-fidelity learning further reduces the computational costs as the pre-training is independent of the potentially expensive evaluations of the actual system of interest, which has typically high-dimensional states.

The manuscript is organized as follows. In Section 2, we define the setup and provide a

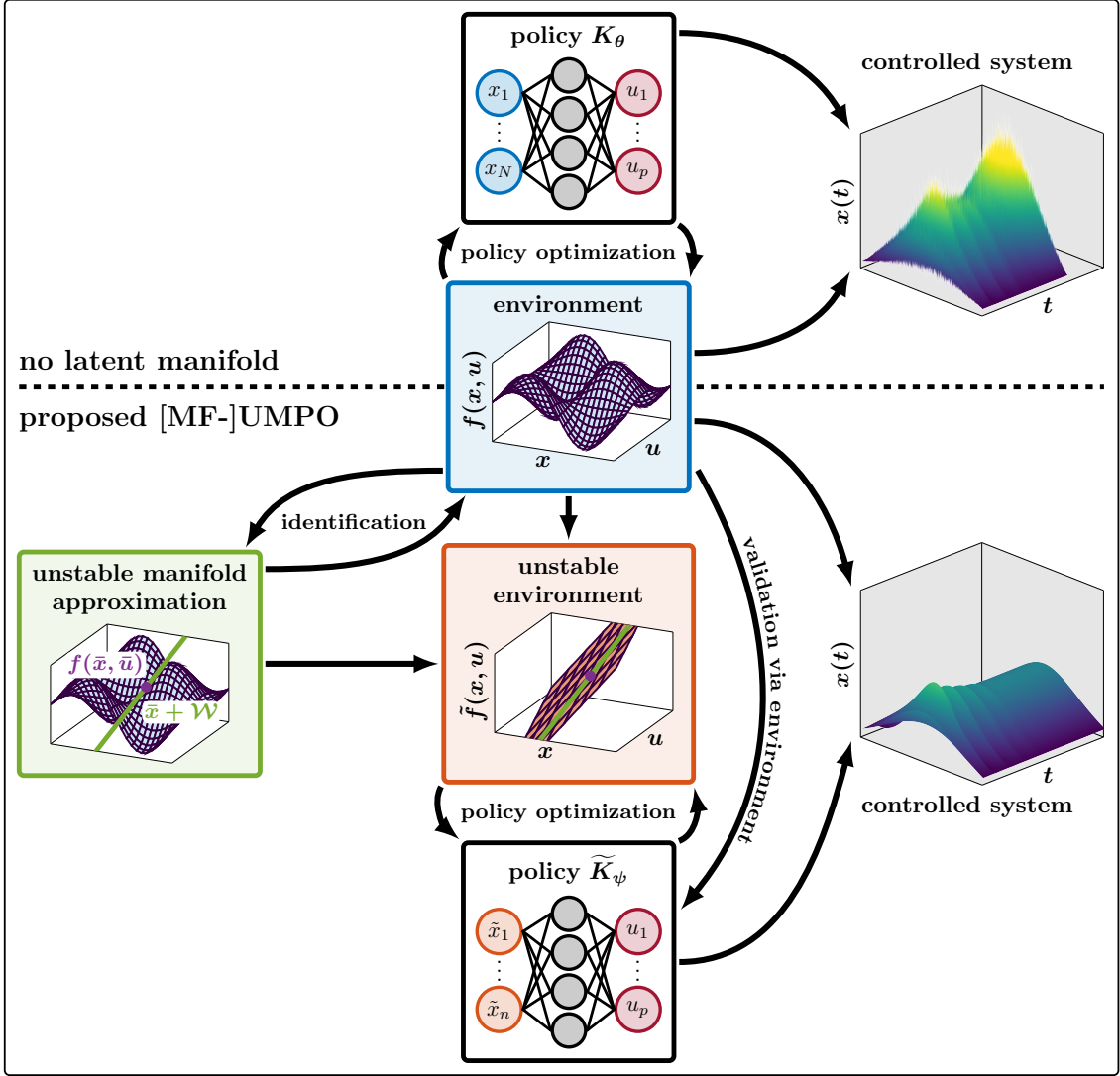


Figure 1: Reinforcement learning methods that optimize policies without unstable manifolds (shown above the dashed line) directly query the dynamical environment in its original, high-dimensional state representation. In contrast, the new [MF-]UMPO methods (shown below the dashed line) consider the dynamics over the low-dimensional unstable manifold instead, which reduces the dimension over which the policy optimization has to act and it reduces the complexity of the task at hand by ignoring dynamical behavior that is irrelevant for stabilization.

problem formulation. We then show in [Section 3](#) that latent manifolds that were trained to generically approximate the system dynamics can be inefficient for stabilization. Our approach is introduced in [Section 4](#) and numerical experiments are shown in [Section 5](#). The work is concluded in [Section 6](#).

2 Stabilizing dynamical systems

In this section, we first introduce the setup for this work before we provide a problem formulation.

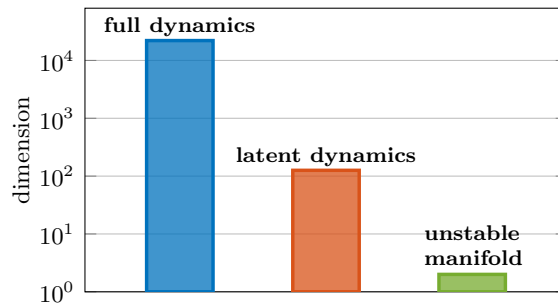


Figure 2: Unstable manifolds can have much lower dimension than standard latent manifolds: For the flow past a cylinder described by the Navier-Stokes equations, the dimension of the unstable manifold is orders of magnitude lower than of a manifold that generically approximates latent dynamics; see [71].

2.1 Setup

We denote discrete-time dynamical systems as

$$x(t+1) = f(x(t), u(t)), \quad t \in \mathbb{N} \cup \{0\}, \quad (1)$$

with initial condition $x(0) \in \mathcal{X}_0 \subseteq \mathbb{R}^N$, N -dimensional internal states $x(t) \in \mathbb{R}^N$ and p -dimensional external control $u(t) \in \mathbb{R}^p$. The function f can be nonlinear in both arguments. The task that we consider here is the construction of a policy K that maps the state $x(t)$ to an input $u(t)$ so that the system (1) is locally stabilized towards a desired equilibrium point (\bar{x}, \bar{u}) for which we have $\bar{x} = f(\bar{x}, \bar{u})$. That is, the closed-loop system

$$x(t+1) = f(x(t), K(x(t)))$$

converges to the steady state $x(t) \rightarrow \bar{x}$ in the limit $t \rightarrow \infty$, if the initial state $x(0)$ lies close enough to the steady state \bar{x} with $\|x(0) - \bar{x}\| \leq \epsilon$ for an $\epsilon > 0$. Notice that in the context of control, the policy K is typically referred to as state-feedback controller. For the construction of the policy K , we can query the system (1) at admissible initial conditions $x(0) \in \mathcal{X}_0$ and control trajectories $u(0), u(1), \dots, u(t_f - 1)$ to observe state trajectories $x(1), x(2), \dots, x(t_f)$ up to some final time t_f .

2.2 Problem formulation

For stabilization via reinforcement learning, we introduce a reward function $r: \mathbb{R}^N \times \mathbb{R}^p \rightarrow \mathbb{R}$ so that $r(x(t), u(t))$ penalizes the distance of $x(t)$ and $u(t)$ from the considered steady state (\bar{x}, \bar{u}) . We parametrize the policy $K_\theta: \mathbb{R}^N \rightarrow \mathbb{R}^p$ over the set of M -dimensional parameters $\Theta \subseteq \mathbb{R}^M$ and we then seek an M -dimensional parameter $\theta_* \in \Theta$ that maximizes the accumulated reward:

$$\theta_* \in \arg \max_{\theta \in \Theta} \sum_{t=0}^{t_f} r(x(t), K_\theta(x(t))). \quad (2)$$

This is a challenging problem. First, because the task is stabilization, we reasonably expect the open-loop system (1) without policy to be unstable and therefore it can be queried only for a short time before instabilities are triggered. Thus, collecting state trajectories is limited due to the instability. In fact, policies K_θ corresponding to intermediate parameters

θ during the optimization process typically lead to destabilization, which makes data collection even more challenging. Second, simulating or querying the system (1) can be expensive. Third, the number of components M of θ typically grows with the complexity of the dynamics described by the system (1); in particular with the state dimension N and the number of control inputs p . Therefore, the search space Θ can be rich and thus large amounts of data are typically required to find informative search directions.

3 Learning on the manifold of unstable dynamics

We propose to learn a low-dimensional manifold in which the dynamics of the system (1) evolve that are important for stabilization, and then to learn a policy K_θ for dynamics on the manifold only. The key insight is that latent manifolds that are typically used for finding low-dimensional latent models and model reduction (e.g., via training autoencoders on state trajectories or even just computing the principal components) are poorly suited for stabilization and instead one should restrict the system to the manifold of unstable dynamics that captures exactly those dynamics that are relevant for the task of stabilization.

3.1 Stabilization on latent manifolds

We denote a latent manifold of the N -dimensional state space of system (1) as

$$\mathcal{M} = \{(D \circ E)(z) : z \in \mathbb{R}^N\}, \quad (3)$$

which is defined via the encoder $E: \mathbb{R}^N \rightarrow \mathbb{R}^n$ and decoder $D: \mathbb{R}^n \rightarrow \mathbb{R}^N$. To give a brief outlook, in Section 4.1, we will learn a policy $\tilde{K}_\psi: \mathbb{R}^n \rightarrow \mathbb{R}^p$ that acts on n -dimensional elements of the encoded manifold $E(\mathcal{M})$ such that $K_\psi = \tilde{K}_\psi \circ E$ stabilizes the high-dimensional system (1); at least locally about the steady state (\bar{x}, \bar{u}) . The parametrization $\psi \in \Psi \subseteq \mathbb{R}^m$ of \tilde{K}_ψ is independent of the dimension N of the high-dimensional state $x(t)$ and instead depends on the dimension n of the manifold \mathcal{M} . In the case that $n \ll N$, this reduces the search space of admissible parametrizations from Θ with dimension M to Ψ with dimension $m \ll M$ and, consequently, the computational costs of learning K_ψ .

In Section 4.2, we will go one step further and additionally restrict the system dynamics of (1) onto \mathcal{M} by considering the states $\tilde{x}(t) \in \mathbb{R}^n$ with dimension $n \ll N$ given by the latent model

$$\tilde{x}(t+1) = E \circ f(D(\tilde{x}(t)), u(t)), \quad (4)$$

Then, the policy \tilde{K}_ψ will be trained on the latent model (4), which avoids having to query the potentially more expensive, high-dimensional model (1). However, additional conditions on E and D are necessary such that the dynamics described by (4) are informative enough for the stabilization of (1) by $K_\psi = \tilde{K}_\psi \circ E$. Additionally, due to computational inexactness, limited data and the finite-dimensional parametrizations of the complex manifolds that hold the dynamics important for stabilization, one can trust the latent model (4) in actual numerical computations only in limited cases and, therefore, recourse to the high-dimensional model (1) will certify the stabilization; see multi-fidelity methods [51, 70].

3.2 Why not every latent manifold is a good choice for stabilization

We now discuss that latent manifolds \mathcal{M} that describe well essential system dynamics so that the states $\tilde{x}(t)$ of the latent model (4) approximate the states $x(t)$ of the high-dimensional model (1) can still lead to catastrophic errors when used for stabilization.

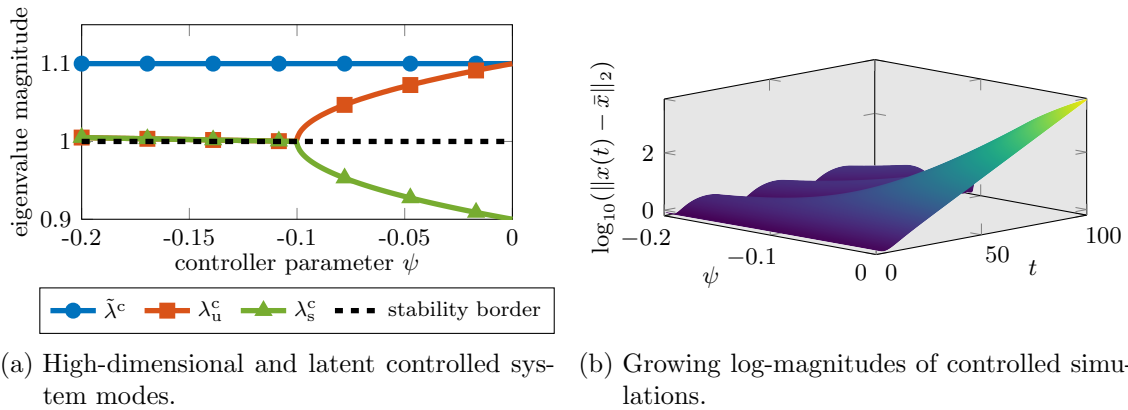


Figure 3: PCA subspaces are insufficient for stabilization: While the latent model created from a fully converged low-dimensional PCA subspace has the same unstable eigenvalue as the true system, its controlled behavior does not coincide with the true system steered via the corresponding decoded policy, since the controlled latent eigenvalue $\tilde{\lambda}^c$ does not change, while the controlled true eigenvalues λ_u^c and λ_s^c do (see (a)). Tuning the policy parameter ψ does not stabilize the true system since λ_u^c and λ_s^c do not decrease below the stability border and the simulation trajectories (see (b)) do not converge to the steady state but oscillate or even grow in magnitude.

A well-known approach to compute suitable latent manifolds to approximate the system dynamics in the special case of linear systems is the balanced truncation method [44]. However, the system needs to be known for this method and only under strict assumptions, these manifolds are suitable for the task of stabilization [8, 45]. In the following, we consider the sampling-based approach of principal components, which can lead to good approximations of the system dynamics in general but either ignore or overfit the unstable behavior.

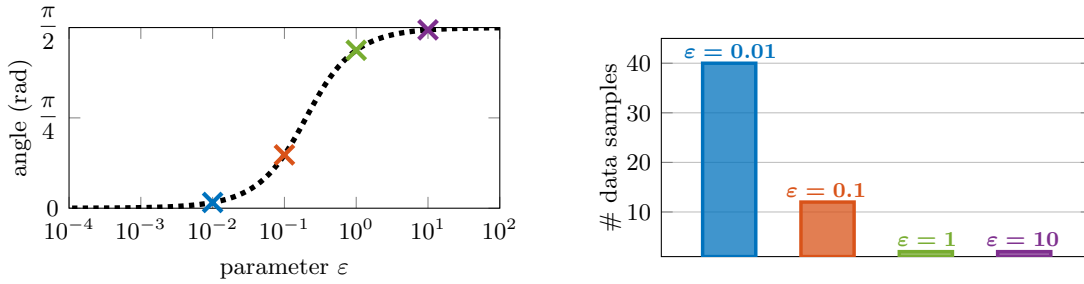
Principal components can lead to unsuitable latent manifolds for stabilization. A classical approach to find a suitable manifold \mathcal{M} for the system dynamics of (1) is to train the manifold so that the embedding error $\|(D \circ E)(x(t)) - x(t)\|$ is small. We consider the linear manifold of dominant dynamics \mathcal{V} that minimizes the embedding error, which is given by the principal component analysis (PCA) [48, 57, 66]. We collect the principal components as orthogonal columns in $V \in \mathbb{R}^{N \times n}$ to obtain the encoder and decoder as

$$D_{\mathcal{V}}(\tilde{x}(t)) = V\tilde{x}(t) \quad \text{and} \quad E_{\mathcal{V}}(x(t)) = V^T x(t).$$

We use principal components just for ease of exposition here in this motivating example but the insights apply to nonlinear embeddings as well. Consider the linear system $x(t+1) = f(x(t), u(t)) = Ax(t) + Bu(t)$ given by

$$A = \begin{bmatrix} 0.9 & 0 \\ \varepsilon & 1.1 \end{bmatrix}, \quad B = \begin{bmatrix} 1 \\ 0 \end{bmatrix}, \quad x(0) = \begin{bmatrix} 0 \\ 0 \end{bmatrix}, \quad (5)$$

with $\varepsilon > 0$. The system in (5) has one stable and one unstable eigenvalue (system mode), where the parameter ε allows to adjust the strength of the coupling between the corresponding dynamics. Mathematically, the strength of the coupling corresponds to the angle between the left and right eigenspaces of the unstable eigenvalue. A small angle means



(a) Distance between PCA and unstable manifold. (b) Number of data samples for PCA to find instability.

Figure 4: Increasing the distance between the PCA and the manifold of unstable system dynamics makes the PCA manifold less suited for the task of stabilization. Via the dynamics coupling in this example (5), the number of data samples needed to identify any instabilities on the PCA manifold increases by $20\times$ from $\varepsilon = 0.01$ to $\varepsilon = 10$.

that principal components mostly ignore the directions in which the system gets unstable; a larger angle means that unstable directions are captured by principal components but result in unwanted influence of the policy on the stable directions, even leading to destabilization of that system component. The policy for the latent model is parametrized via $\tilde{K}_\psi(\tilde{x}) = \psi\tilde{x}$, with the policy parameter $\psi \in \mathbb{R}$. For $\varepsilon = 0.1$, Figure 3 illustrates that no policy formulated over the PCA subspace is capable of stabilizing the true system (5) of interest. This can be seen clearly in Figure 3b where for none of the policy parameters ψ , the trajectories converge to the steady state \bar{x} but rather oscillate or even diverge indicated by the growing magnitudes. The underlying problem with the PCA-based manifold is revealed in Figure 3a. The eigenvalues of the controlled systems shown here are denoted by

$$\tilde{\lambda}^c = \Lambda(\tilde{J}_x + \tilde{J}_u \tilde{K}_\psi(1)) \quad \text{and} \quad \{\lambda_s^c, \lambda_u^c\} = \Lambda(A + B\tilde{K}_\psi \circ E_{\mathcal{V}}(I_2)),$$

where $\tilde{J}_x = V^T A V$, $\tilde{J}_u = V^T B$, $E_{\mathcal{V}}(I_2)$ denotes the column-wise application of $E_{\mathcal{V}}$ to the two-dimensional identity matrix I_2 , and λ_s^c and λ_u^c correspond to the stable and unstable eigenvalues of the original system (5), respectively. While the corresponding latent model that lives on \mathcal{M} has the same unstable system mode as the original system (5), the influence of policies on the latent model corresponding to PCA appears to be strongly different from its effect on the true system. In fact, there is no visible area in Figure 3a in which both the controlled eigenvalues λ_u^c and λ_s^c decrease below the stability border, which would indicate the stability of the true controlled system by the low-dimensional policy, and the latent model mode $\tilde{\lambda}^c$ is stabilized in a different region of the parameter ψ that is not shown in Figure 3a. Due to monotonicity of the system modes, the true system of interest cannot be stabilized in the parameter region, where the latent model is stabilized, and vice versa.

Large amounts of data are required to compensate for poorly suited latent manifolds.

Not targeting the unstable dynamics directly translates into requiring large amounts of trajectory data to capture the dynamics necessary for stabilization. Even when PCA captures the unstable dynamics eventually, building a policy in the PCA subspace can lead to a pollution effect in the sense that the learned policy also affects stable dynamics in undesired ways as shown in Figure 3; see [72]. Figure 4 shows the distance between the PCA-based manifold of system dynamics and the manifold of unstable dynamics, which

is needed for the design of stabilizing policies, and the corresponding amounts of data needed for PCA to identify any instability. With increasing distance between the two manifolds, given in terms of subspace angles in Figure 4a, the PCA becomes less suitable for the design of stabilizing policies as the amount of data needed to identify instabilities increases; see Figure 4b. Sometimes this can be compensated using even more data samples in the learning process of the policy, but there are no guarantees as, for example, Figure 3 indicates that there is no stabilizing policy on the PCA manifold.

3.3 The latent manifold of unstable dynamics

We propose to consider the dynamics relevant for the task of stabilization, which means the purely unstable system dynamics, instead of aiming to find a latent manifold \mathcal{M} that approximates all system dynamics in general. The manifold of unstable dynamics about the steady state (\bar{x}, \bar{u}) is defined as

$$\mathcal{M}_u(\bar{x}, \bar{u}) = \left\{ x(t) \in \mathbb{R}^N : \lim_{t \rightarrow \infty} \phi^{-t}(x(t)) = \bar{x} \text{ for } u(t) = \bar{u} \right\}, \quad (6)$$

where ϕ^{-t} is the inverse flow map of (1) that goes backwards in time [34, 75]. Thus, the manifold $\mathcal{M}_u(\bar{x}, \bar{u})$ includes the trajectories that originate arbitrarily close to the steady state (\bar{x}, \bar{u}) but can diverge from it over time. For the low-dimensional representation of the unstable manifold (6), we need to find encoder E and decoder D that fully characterize its dynamics. Therefore, the time evolution in (4) is the restriction of the states $x(t)$ such that $\tilde{x}(t) = E(x(t))$ holds for all $x(t) \in \mathcal{M}_u$. This exact representation yields the equation

$$E(x(t+1)) = E \circ f((D \circ E)(x(t)), u(t)).$$

Inserting this into the encoding of the high-dimensional system (1) results in the following condition to hold for the encoder and decoder in terms of the system dynamics and states:

$$E \circ f(x(t), u(t)) = E \circ f((D \circ E)(x(t)), u(t)), \quad (7)$$

for all $x(t) \in \mathcal{M}_u(\bar{x}, \bar{u})$. Since we consider local stabilization with the states $x(t) \in \mathcal{M}_u$ satisfying $\|x(t) - \bar{x}\| \leq \epsilon$ for some $\epsilon > 0$, and under the assumption that the function f in (1) is analytic in both arguments, the linearization of f about (\bar{x}, \bar{u}) given via its Taylor series expansion will yield sufficient information about the dynamics:

$$f(x(t), u(t)) = f(\bar{x}, \bar{u}) + J_x(x(t) - \bar{x}) + J_u(u(t) - \bar{u}) + \mathcal{O}((x(t) - \bar{x})^2) + \mathcal{O}((u(t) - \bar{u})^2),$$

where $J_x(x) = (\nabla_x f(\bar{x}, \bar{u}))x$ is the Jacobian of f with respect to the state and $J_u(u) = (\nabla_u f(\bar{x}, \bar{u}))u$ is the Jacobian of f with respect to the input. Since (\bar{x}, \bar{u}) is an equilibrium point, we have that $\bar{x} = f(\bar{x}, \bar{u})$. Therefore, by introducing the new state and input variables $\tilde{x}(t) = x(t) - \bar{x}$ and $\tilde{u}(t) = u(t) - \bar{u}$ that describe the deviation from the desired system behavior in (1) yields

$$x(t+1) - \bar{x} = \tilde{x}(t+1) = J_x(\tilde{x}(t)) + J_u(\tilde{u}(t)) + \mathcal{O}(\tilde{x}(t)^2) + \mathcal{O}(\tilde{u}(t)^2).$$

About (\bar{x}, \bar{u}) , the original system (1) is well approximated by

$$\tilde{x}(t+1) = J_x(\tilde{x}(t)) + J_u(\tilde{u}(t)). \quad (8)$$

Note that $(0, 0)$ is the steady state of (8) that corresponds to (\bar{x}, \bar{u}) in (1). Inserting (8) into the condition (7) and making the linear ansatz

$$E_{\mathcal{W}}(x(t)) = W^T x(t) \quad \text{and} \quad D_{\mathcal{W}}(\tilde{x}(t)) = (W^T)^\dagger \tilde{x}(t), \quad (9)$$

with $W \in \mathbb{R}^{N \times n}$, for the encoder and decoder results in the invariant subspace equation

$$W^\top J_x = \left(W^\top J_x (W^\top)^\dagger \right) W^\top, \quad (10)$$

where the eigenvalues of $(W^\top J_x (W^\top)^\dagger)$ are all the eigenvalues of J_x with absolute value larger or equal to one. The basis matrix W spans the subspace \mathcal{W} such that $\bar{x} + \mathcal{W}$ yields an exact description of \mathcal{M}_u in the steady state of interest (\bar{x}, \bar{u}) and is expected to be a suitable approximation for the rest of the dynamics $x(t) \in \mathcal{M}_u(\bar{x}, \bar{u})$ with $\|x(t) - \bar{x}\| \leq \epsilon$; see [34, 71, 75]. Also, note that the subspace \mathcal{W} has the same dimension n as the manifold $\mathcal{M}_u(\bar{x}, \bar{u})$, which only increases with the number of unstable eigenvalues of the Jacobian J_x in the steady state. In other words, the dimension only depends on the number of unstable system modes, which is independent of the state dimension N and the dimension p of the controls; see Figure 2.

3.4 Estimation of encoders and decoders from adjoint data

For the construction of the encoder $E_{\mathcal{W}}$ in (9) from data, we observe that (10) defines the basis matrix W via a linear left eigenvalue equation in matrix form [21]. Therefore, the unstable manifold about the steady state is described by the left eigenvectors corresponding to the unstable eigenvalues of J_x . The estimation of the left eigenvalues and eigenvectors of the Jacobian of f is possible via adjoint data, which can be obtained in a non-intrusive way [20, 31, 50] via automatic differentiation of f with respect to $x(t)$. In particular, the eigenvectors are estimated using data obtained by querying the adjoint system on initial conditions and observing the state trajectories. Many modern code packages allow for the use of automatic differentiation like JAX [10], FEniCS DOLPHIN [42], TensorFlow [1] and PyTorch [47]. To generate data from the adjoint system, we consider the idea of reverse accumulation also known as adjoint mode automatic differentiation. Reverse accumulation allows for vector-Jacobian products of the form

$$F[\bar{x}, \bar{u}](z) = z^\top J_x = z^\top \nabla_x f(\bar{x}, \bar{u}),$$

for $z \in \mathbb{R}^N$, which is equivalent to querying the adjoint system given by the adjoint operator

$$G[\bar{x}, \bar{u}](z) = (F[\bar{x}, \bar{u}](z))^\top = J_x^\top z = (\nabla_x f(\bar{x}, \bar{u}))^\top z. \quad (11)$$

The left eigenspaces of J_x given by the operator F are the right eigenspaces of J_x^\top given by the operator G . Notice that the eigenvectors are computed using only queries of the operator on vectors, which are given by state observations. Thereby, we can compute the left eigenspaces in (10) by evaluating the adjoint system (11) using vector-Jacobian products in Krylov methods [4, 63].

4 Leveraging the latent manifold of unstable dynamics for reinforcement learning

In this section, we introduce unstable manifold policy optimization (UMPO) to optimize for a policy that acts on the latent states of the manifold of unstable dynamics. We further introduce multi-fidelity policy optimization (MF-UMPO) that combines optimizing for a policy with a latent model over the unstable manifold and subsequently correcting the policy with the high-dimensional state model.

4.1 Policy optimization on unstable manifolds

We now leverage the approximation of the unstable latent manifold $\bar{x} + \mathcal{W}$ to train a policy K_ψ with a low-dimensional parametrization for stabilizing the high-dimensional system (1). We denote this method as UMPO. Thereby, we first learn $\tilde{K}_\psi : \mathbb{R}^n \rightarrow \mathbb{R}^p$ that is parametrized over $\Psi \subseteq \mathbb{R}^m$ and that acts on latent states of dimension n . Then, we lift \tilde{K}_ψ via the encoder $E_{\mathcal{W}}$ of the unstable latent manifold \mathcal{M}_u to act on states $x(t)$ of the high-dimensional system (1),

$$K_\psi(x(t)) = \tilde{K}_\psi(E_{\mathcal{W}}(x(t) - \bar{x})) + \bar{u}, \quad (12)$$

where a shift by the equilibrium point (\bar{x}, \bar{u}) is added to center the unstable manifold \mathcal{M}_u at the steady state \bar{x} and the control signals at the steady-state control \bar{u} . The parameter vector ψ of K_ψ can then be trained with an objective such as (2) by querying the high-dimensional system (1) using, e.g., policy gradient methods (DDPG [37], TD3 [18]) that are suited for continuous observation and action spaces.

In contrast to direct approaches that learn K_θ by acting on the N -dimensional states $x(t)$ of the high-dimensional system (1), the policy K_ψ given in (12) includes an encoding step with $E_{\mathcal{W}}$ that maps the shifted $x(t)$ onto a low-dimensional latent state of dimension n . Thus, the parametrization $\Psi \subseteq \mathbb{R}^m$ of K_ψ depends on the dimension of the unstable latent manifold n , in contrast to $\Theta \subseteq \mathbb{R}^M$ of K_θ that depends on the dimension N of the high-dimensional model (1). Due to the change in the dimensions of the policy mapping, a lower dimensional parametrization $m \ll M$ is sufficient for K_ψ than for K_θ , which reduces the optimization space and training costs, as we will demonstrate with numerical experiments below. The UMPO method is summarized in Algorithm 1 for the case of *no multi-fidelity* using Lines 1, 6 and 8.

4.2 Multi-fidelity policy optimization on the unstable manifold

We now propose a multi-fidelity version of UMPO, where an policy is pre-trained on a cheap-to-evaluate surrogate latent model of the system dynamics of interest so that the pre-trained policy is a good starting point for easing the training on the high-dimensional system (1). Additionally, because the agent is trained on the high-dimensional model eventually, confidence in the learned policy can be higher than when learning with a surrogate model alone.

Latent model of unstable dynamics for pre-training. The latent model of unstable dynamics is given by

$$\tilde{x}(t+1) = \tilde{J}_x(\tilde{x}(t)) + \tilde{J}_u(\tilde{u}(t)), \quad (13)$$

with the state transition and control terms

$$\tilde{J}_x(\tilde{x}(t)) = E_{\mathcal{W}}(\nabla_x f(\bar{x}, \bar{u})D_{\mathcal{W}}(\tilde{x}(t))) \quad \text{and} \quad \tilde{J}_u(\tilde{u}(t)) = E_{\mathcal{W}}(\nabla_u f(\bar{x}, \bar{u})\tilde{u}(t)), \quad (14)$$

where the encoder $E_{\mathcal{W}}$ and decoder $D_{\mathcal{W}}$ are defined in (9). This is a specific instance of the generic latent model given in (4) that results from applying the chosen encoder and decoder (7) to the linearized dynamics in (8). As \tilde{J}_x and \tilde{J}_u in (13) are linear, the describing matrices can be assembled using the reverse mode automatic differentiation as in the estimation of \mathcal{W} in Section 3.4. The terms (14) can then be computed by

$$\tilde{J}_x = E_{\mathcal{W}}(\nabla_x f(\bar{x}, \bar{u}))(W^T)^\dagger \quad \text{and} \quad \tilde{J}_u = E_{\mathcal{W}}(\nabla_u f(\bar{x}, \bar{u})), \quad (15)$$

where $E_{\mathcal{W}}(\cdot)$ above is applied column-wise to the argument and $(W^T)^\dagger$ comes from the decoder $D_{\mathcal{W}}$ in (9). Alternatively, the terms in (13) can be learned via $n + p$ forward evaluations of (1) and system identification in the subspace \mathcal{W} ; see [72, Prop. 1]. This can be advantageous compared to (15) because it allows to separate the computational steps for estimating \mathcal{W} and (13), which is important in modularized implementations. In any case, the terms in (14) for (13) can be precomputed and stored as matrices, which means that querying the latent model of unstable dynamics (13) is cheap, and thus well suited for pre-training in a first step of multi-fidelity reinforcement learning.

Multi-fidelity fine-tuning on the unstable manifold. We now propose multi-fidelity policy optimization with the unstable latent manifold (MF-UMPO), which proceeds in two steps. In Step 1, the policy \tilde{K}_ψ with parametrization $\psi \in \Psi$ as defined in (12) is pre-trained to stabilize the latent model of unstable dynamics (13) with respect to the equilibrium point $(0, 0)$. The result is a parameter ψ_*^{pre} that is pre-trained using the latent model only. In Step 2, the pre-trained parameter ψ_*^{pre} is used as starting point for training the policy $\tilde{K}_{\psi_*^{\text{pre}}}$ defined in (12) on the high-dimensional system (1) to obtain ψ_* with the procedure described in the previous paragraph. The corresponding policy K_{ψ_*} is then used for stabilizing the high-dimensional model (1).

Key is that the pre-trained ψ_*^{pre} is a good starting point for Step 2, so that fine-tuning in a multi-fidelity sense [51, 70] is cheap in terms of, e.g., high-dimensional model queries. In particular, the pre-trained parameter vector ψ_*^{pre} has to be an admissible point in the sense that it locally stabilizes the high-dimensional system (1) when used in (12). The MF-UMPO method is summarized in Algorithm 1.

The following theorem shows that the parameter ψ_*^{pre} obtained via the pre-training yields an admissible, stabilizing policy for the high-dimensional system (1).

Theorem 1. *Let f in (1) be analytic in (\bar{x}, \bar{u}) and let the parameter ψ_*^{pre} be such that the policy $\tilde{K}_{\psi_*^{\text{pre}}}$ is stabilizing for (13) with respect to the zero steady state $(0, 0)$. Then, there exists an epsilon $\epsilon > 0$ such that $\tilde{K}_{\psi_*^{\text{pre}}}$ in the control law (12) is locally stabilizing for (1) for all initial values $x(0) \in \mathcal{X}_0$ such that $\|x(0) - \bar{x}\| \leq \epsilon$.*

Proof. From the assumptions, it follows that the Taylor series expansion of f about (\bar{x}, \bar{u}) yields a suitable approximation of the dynamics of (1) via the linear system (8). From the condition that ψ_*^{pre} is such that the policy $\tilde{K}_{\psi_*^{\text{pre}}}$ is stabilizing for (13) and the fact that the encoder and decoder in (9) are constructed via the basis matrix W of the left eigenspace corresponding to the unstable eigenvalues of J_x , it follows from [71, Lem. 1] that the policy $K_{\psi_*^{\text{pre}}}$ with (12) is stabilizing for (8) towards the $(0, 0)$ steady state. Then it follows from [71, Prop. 1] that there exists an $\epsilon > 0$ such that $K_{\psi_*^{\text{pre}}}$ is locally stabilizing for the equilibrium (\bar{x}, \bar{u}) in (1), which proves the result of the theorem. \square

Following Theorem 1, we see that the initialization of the neural network in (12) with ψ_*^{pre} for the training on (1) yields an admissible policy that just needs to be adjusted to the high-dimensional system (1).

4.3 Algorithmic description

Algorithm 1 summarizes the steps for learning stabilizing policies on the unstable manifold with an optional pre-training step on the latent model of unstable dynamics. As the first step of Algorithm 1 in Line 1, the basis matrix W for the encoder and decoder is learned via vector-Jacobian products with the operator f as described in Section 4.1.

Algorithm 1: [Multi-fidelity] Unstable manifold policy optimization ([MF-]UMPO).

-
- Input:** Steady state (\bar{x}, \bar{u}) , queryable model f .
Output: Parameters ψ_* for policy K_ψ in (12).
- 1 Estimate the the left unstable eigenspace \mathcal{W} in (10) using vector-Jacobian products with f in (\bar{x}, \bar{u}) and a Krylov eigenvalue solver.
 - 2 **if** *multi-fidelity* **then**
 - 3 Learn the low-dimensional model $(\tilde{J}_x, \tilde{J}_u)$ of unstable dynamics (13) using:
 - (a) automatic differentiation of f , or
 - (b) system identification with $n + p$ forward evaluations of f .
 - 4 Obtain a parameter ψ_*^{pre} by training \tilde{K}_ψ to be a stabilizing policy for (13) with respect to the $(0, 0)$ steady state.
 - 5 **else**
 - 6 Set the parameter initialization ψ_*^{pre} to be random.
 - 7 **end**
 - 8 Obtain the parameter ψ_* by training K_ψ in (12) to be a stabilizing policy for (1) with the initialization ψ_*^{pre} .
-

Afterwards, if the optional pre-training is desired (determined via the flag *multi-fidelity* in Algorithm 1), the latent model of unstable dynamics (13) is learned using the basis matrix W from the previous step and either automatic differentiation of f or classical system identification via forward evaluations of f . Once the matrices in (13) are known, this latent model is used in a policy optimization loop to obtain a policy $\tilde{K}_{\psi_*^{\text{pre}}}$ that stabilizes (13) towards the $(0, 0)$ steady state. Using (13) for the policy optimization yields the two main advantages compared to using directly (1), namely that (i) the latent model is cheaper to evaluate since $n \ll N$, and (ii) the dynamics of (1) are easier to stabilize since they are purely unstable and the training does not destabilize any additional dynamics that have been stable before. Also note that $\tilde{K}_{\psi_*^{\text{pre}}}$ follows the theory in Theorem 1 such that it is an admissible, stabilizing policy for the high-dimensional problem already. In the case that no pre-training is requested, the initial parametrization is set to be random.

Lastly, in Line 8 of Algorithm 1, the initialization ψ_*^{pre} is fine tuned via policy optimization on the high-dimensional system. In the case without pre-training, this step learns a stabilizing policy from scratch while in the multi-fidelity version, an admissible policy is verified on the high-dimensional system and further improved in terms of its final performance.

5 Numerical experiments

We demonstrate UMPO and MF-UMPO with three numerical experiments. The reported experiments were run on compute nodes of the **Greene** high-performance computing cluster of the New York University equipped with 16 processing cores of the Intel Xeon Platinum 8268 24C 205W CPU at 2.90 GHz and 16, 32 or 48 GB main memory. We implemented the experiments in Python 3.9.12 running on Red Hat Enterprise Linux release 8.4 (Ootpa). For the reinforcement learning agents, we use the DDPG implementation from JAXRL version 0.0.7 [30]. The source codes, data and computed results of the experiments are available at [69].

5.1 Setup of numerical experiments

5.1.1 Training rewards

A classical cost function for stabilization via optimal control is given as the sum of the quadratic deviations of the state and the input from the controlled steady state of interest (\bar{x}, \bar{u}) :

$$J(u(t)) = \sum_{t=0}^{t_f} \|x(t) - \bar{x}\|_Q^2 + \|u(t) - \bar{u}\|_R^2,$$

where the weighted norms are given by

$$\|x(t) - \bar{x}\|_Q^2 = (x(t) - \bar{x})^\top Q (x(t) - \bar{x}) \quad \text{and} \quad \|u(t) - \bar{u}\|_R^2 = (u(t) - \bar{u})^\top R (u(t) - \bar{u}),$$

for some symmetric positive semi-definite matrices $Q \in \mathbb{R}^{N \times N}$ and $R \in \mathbb{R}^{p \times p}$; see, for example, [38]. This inspired the use of quadratic reward functions in control-oriented reinforcement learning tasks [22, 24, 36, 39, 43]. In our setup, we employ the reward function

$$r(x(t), u(t)) = -\sqrt{\|x(t) - \bar{x}\|_Q^2 + \|u(t) - \bar{u}\|_R^2}, \quad (16)$$

with the weighting terms to be $Q = I_N$ and $R = \lambda_u I_p$, and the regularization constant $\lambda_u \geq 0$. Additionally, early termination of episodes at a time $t_a < t_f$ due to instabilities, where t_f denotes the episode length, is penalized by approximations of the remaining accumulated rewards as

$$r(x(t_a), u(t_a)) = -\sqrt{(t_f - t_a) \|x(t) - \bar{x}\|_Q^2 + \|u(t) - \bar{u}\|_R^2},$$

to encourage the optimization towards policies with full episode length. In the comparison of the different approaches, we consider a normalized variant of the accumulated rewards (2) per episode given by

$$R_n = \frac{\sum_{j=0}^{t_f} r(x(t), u(t))}{\sqrt{(r + \lambda_u) t_f}}, \quad (17)$$

with episode length t_f , dimension of the observable r and the regularization constant λ_u from (16). Note that the state-space dimension r in (17) is either N for the direct approach or n in the case of the new approaches on the unstable manifold. We observed that the accumulated rewards range between several orders of magnitude, therefore we use in the comparison the logarithmic mean

$$\text{logmean}(R_n) = -10^{\frac{1}{q} \sum_{j=1}^q \log_{10} |R_n^j|},$$

with $q \in \mathbb{N}$, the number of considered elements.

5.1.2 Governing equations of physical models

The examples considered in the following include a nonlinear reaction-diffusion problem modeled by the Allen-Cahn equation [2, 15], a chemical reaction inside a tubular reactor [25, 32] and the behavior of crystal clusters modeled via the Toda lattice [65, 68]. The corresponding equations describing the physical problems and details on the space-time discretizations can be found below. The governing equations are numerically solved with implementations using JAX [10] to enable automatic differentiation with respect to states and controls. The implementations of the models can be found in the accompanying code package [69].

Allan-Cahn equation. This example is a nonlinear reaction-diffusion process described by the one-dimensional Allen-Cahn equation [2]. The particular instance of the equation used here is sometimes also referred to as Chafee-Infante equation [15]. The equation with homogeneous Dirichlet boundary conditions is given by

$$\partial_t \nu(t, \zeta) - \kappa \Delta \nu(t, \zeta) + \alpha_1 \nu(t, \zeta)^3 - \alpha_2 \nu(t, \zeta) + u(t) = 0, \quad \text{for } \zeta \in \Omega, \quad (18a)$$

$$\nu(t, \zeta) = 0, \quad \text{for } \zeta \in \partial\Omega, \quad (18b)$$

with the diffusion parameter $\kappa \in \mathbb{R}$, the two reaction parameters $\alpha_1, \alpha_2 \in \mathbb{R}$ and the distributed controls $u(t)$. For our experiments, the diffusion parameter has been chosen as $\kappa = 0.2$ and the reaction parameters as $\alpha_1 = 2.5$ and $\alpha_2 = 0$. The spatial coordinates of (18) in $\Omega = (0, 1)$ are discretized using a finite difference scheme such that $N = 1000$ and $p = 1$. The system is discretized in time via the implicit-explicit (IMEX) Euler scheme, with sampling time $\tau = 0.01$, where the linear state evolution is considered implicitly and the nonlinear term and the controls explicitly. Note that the terms of the discrete-time system are not computed explicitly but implemented via function evaluations. An output operator C is chosen to generate output channels via $y(t) = Cx(t)$ showing as first entry the accumulated state variables for the first third of the spatial domain and the accumulated rest in the second channel. The steady state of interest is computed using the Newton iteration for the constant steady state control $\bar{u} = 1$. The system has one ($n = 1$) unstable mode in (\bar{x}, \bar{u}) .

Tubular reactor model. The tubular reactor model describes a combustion-based reaction inside a tube that transforms reactants into desired products [25, 32]. The process is described by the one-dimensional coupled partial differential equations

$$\partial_t \psi(t, \zeta) = \frac{1}{\text{Pe}} \Delta \psi(t, \zeta) - \partial_\zeta \psi(t, \zeta) - \mathcal{D} \psi(t, \zeta) e^{\gamma - \frac{\gamma}{\nu(t, \zeta)}}, \quad \text{for } \zeta \in \Omega, \quad (19a)$$

$$\begin{aligned} \partial_t \nu(t, \zeta) &= \frac{1}{\text{Pe}} \Delta \nu(t, \zeta) - \partial_\zeta \nu(t, \zeta) - \beta(\nu(t, \zeta) - \nu_{\text{ref}} u_2(t)) \\ &\quad + \mathcal{B} \mathcal{D} \psi(t, \zeta) e^{\gamma - \frac{\gamma}{\nu(t, \zeta)}}, \end{aligned} \quad \text{for } \zeta \in \Omega, \quad (19b)$$

$$0 = \partial_\zeta \psi(t, \zeta) - \text{Pe}(\psi(t, \zeta) - u_1(t)), \quad \text{for } \zeta \in \partial\Omega_1, \quad (19c)$$

$$0 = \partial_\zeta \nu(t, \zeta) - \text{Pe}(\nu(t, \zeta) - u_2(t)), \quad \text{for } \zeta \in \partial\Omega_1, \quad (19d)$$

$$0 = \partial_\zeta \psi(t, \zeta), \quad \text{for } \zeta \in \partial\Omega_2, \quad (19e)$$

$$0 = \partial_\zeta \nu(t, \zeta), \quad \text{for } \zeta \in \partial\Omega_2, \quad (19f)$$

where $\psi(t, \zeta)$ is the concentration of the reactant and $\nu(t, \zeta)$ the temperature of the tube. The spatial domain is chosen as $\Omega = (0, 1)$, with $\partial\Omega_1 = 0$ and $\partial\Omega_2 = 1$. The parameters in (19) are chosen as in [32] with $\text{Pe} = 5$, $\mathcal{D} = 0.167$, $\gamma = 25$, $\beta = 2.5$, $\nu_{\text{ref}} = 1$ and $\mathcal{B} = 0.5$. The controls in this example allow the change of the reactant concentration at the right end of the tube as well as steering the temperature of the complete tube. The system is discretized in space via finite differences and in time using the IMEX Euler scheme, with the sampling time $\tau = 0.01$, where the linear state contributions are considered implicitly and the nonlinear part and inputs explicitly. If not stated otherwise, the state dimension of this example is $N = 998$ with $p = 2$ control inputs. For the computations in Figure 10, finer discretizations have been used, too. Note that the terms of the discrete-time system are not computed explicitly but implemented via function evaluations. An output operator C is chosen to generate two measurements of the form $y(t) = Cx(t)$ giving the concentration and temperature at the left end of the tube. The steady state of

interest is computed using the Newton iteration for the steady state control $\bar{u} = 1$. For any discretization size discussed here, the system has two ($n = 2$) unstable modes in (\bar{x}, \bar{u}) leading under disturbances to limit cycle oscillations of the state.

Toda lattice model. The Toda lattice model describes the vibrational behavior of a one-dimensional crystal structure [65, 68]. We consider here the process of crystallization, in which particles have formed clusters that repel each other if disturbances occur. The ordinary differential equations describing the process in parametrized form were derived in [68]. A crystal with ℓ particles is given by

$$m_1 \ddot{q}_1(t) + \gamma_1 \dot{q}_1(t) + e^{k_1(q_1(t) - q_2(t))} - 1 = u_1(t), \quad (20a)$$

$$m_j \ddot{q}_j(t) + \gamma_j \dot{q}_j(t) + e^{k_j(q_j(t) - q_{j+1}(t))} - e^{k_{j-1}(q_{j-1}(t) - q_j(t))} = u_j(t), \quad (20b)$$

$$m_\ell \ddot{q}_\ell(t) + \gamma_\ell \dot{q}_\ell(t) + e^{k_\ell q_\ell(t)} - e^{k_{\ell-1}(q_{\ell-1}(t) - q_\ell(t))} = u_\ell(t), \quad (20c)$$

for $j = 2, \dots, \ell - 1$. Therein are $m_i > 0$, $\gamma_i > 0$ and $k_i \in \mathbb{R}$ the mass, damping and particle forces of the i -th particle. The states in (20) are $q_i(t)$ as the displacement of the i -th particle such that $\dot{q}_i(t)$ is the corresponding momentum. The system (20) is described by second-order differential equations. For the design of policies, the system is considered in first-order form using its phase state

$$x(t) = \begin{bmatrix} q(t) \\ \dot{q}(t) \end{bmatrix} \in \mathbb{R}^{2\ell},$$

where $q(t)$ and $\dot{q}(t)$ are the concatenated displacement and momentum vectors of all particles. In our experiments, we have chosen $\ell = 500$ particles such that the considered first-order system has the order $N = 1000$. The parameters in (20) are chosen to model three clusters of sizes (150, 250, 100) with different particles of the form:

$$m = \mathbf{1}_{100}^\top \otimes [2 \quad 1 \quad 3 \quad 5 \quad 4],$$

$$\gamma_j = \begin{cases} 0.1 & \text{for } j < 150, \\ 0.1 & \text{for } j = 150, \\ 0.15 & \text{for } 150 < j < 400, \\ 0.1 & \text{for } j = 400, \\ 0.5 & \text{for } 400 < j \leq 500, \end{cases}$$

$$k_j = \begin{cases} 2 & \text{for } j < 150, \\ -1 & \text{for } j = 150, \\ 5 & \text{for } 150 < j < 400, \\ -2 & \text{for } j = 400, \\ 1 & \text{for } 400 < j \leq 500. \end{cases}$$

The negative forces for the particles at the end of the clusters result in repulsion between the clusters. The controls allow to influence the displacement of all particles inside a cluster such that $p = 3$. The system is discretized in time with the same IMEX Euler scheme that is used for the other examples such that the linear state evolution is handled implicitly and the nonlinearity and inputs explicitly, with sampling time $\tau = 0.1$. Note that the terms of the discrete-time system are not computed explicitly but implemented in function evaluations. An output operator C is chosen to generate three measurements via $y(t) = Cx(t)$ giving the mean velocity of all particles in a cluster. The zero steady state

Table 1: Sets of hyperparameters used in the experiments. The first three parameters are not varied and fixed for all experiments and all examples. For the rest, experiments have been performed for each possible parameter combination. For the regularization parameter λ_u , we implemented two sets where the first one is used for Allen-Cahn and the tubular reactor examples and the second one for the Toda lattice example.

Maximum number of training steps	10^5
Offline phase steps before training	256
Noise on initial condition	0
Learning rate for actor	{0.005, 0.001, 0.0005, 0.0001}
Learning rate for critic	{0.005, 0.001, 0.0005, 0.0001}
Exploration noise	{0.001, 0}
Episode length t_f	{100, 200, 500}
Regularization parameter λ_u	{1000, 0.001, 0} or { 10^6 , 10^5 , 10^4 }

$(0, 0)$ is considered here for stabilization. The resulting system has two ($n = 2$) unstable modes in (\bar{x}, \bar{u}) , which model the system behavior that particle clusters drift indefinitely apart under small disturbances.

5.1.3 Hyperparameters and learning architectures

We test three variants of the introduced approach: UMPO and MF-UMPO as described in [Algorithm 1](#), and the policy given from the initial parametrization for MF-UMPO, which is learned only on the manifold approximation (13), further denoted by UMPO-MA. These are compared to directly learning a stabilizing policy on the high-dimensional system states denoted by direct DDPG. Further details concerning the setup as well as computational parameters and used neural network architectures can be found below.

Neural network architectures. We implemented DDPG reinforcement learning agents using neural networks for the actors, which approximate the desired policies, and critics, which are needed in the optimization procedure and correspond to the value function; see, for example, [64]. All actors in the experiments are parametrized by neural networks with two hidden layers with ReLU activation functions. The final layer of the networks however uses either `tanh`, `identity` or `ELU`, with parameter $\alpha = 1$, as activation function. Note that the use of `tanh` for control-oriented neural networks is a classical choice [37], which is one motivation for the use of policy parametrizations (12) that are centered around the steady state control \bar{u} . For the critics, the standard architecture from JAXRL [30] has been used. We also experimented with networks with different widths, namely networks with either (20, 10) neurons or (400, 300) neurons in the hidden layers.

Choices of hyperparameters. We performed experiments with fixed random seeds for the initialization of the neural networks and varied the hyperparameters of the learning algorithms. [Table 1](#) shows an overview about the considered parameters in the experiments. For each possible selection from the parameter sets, an experiment has been performed for each example. The last parameter λ_u has two sets, where the first one is used in the Allen-Cahn and tubular reactor examples and the second one in the Toda lattice example. Together with the variations in the neural network architectures, 1 728 experiments have

been run per example and for each of the four presented methods. Some of the hyperparameters in Table 1 have been fixed for all experiments. The maximum number of training steps is fixed for comparability between the experiments, and for variations in the number of offline steps, no noticeable difference in the results has been observed. We apply some noise to the initial condition when resetting a training episode to allow the agent to explore and be trained in different scenarios. However, we have observed that the general inability of neural networks to approximate constants, in particular the zero, has a similar effect as initial noise, especially in the early stages of the training. Additional experiments have been performed to investigate the influence of the state-space dimension N on the training time as shown in Figure 10. For these experiments, we reduced the number of considered hyperparameters by allowing for the learning rates of actor and critic only $\{0.001, 0.0001\}$. This enabled us to fully run the 10^5 training steps also for the direct DDPG approach.

5.2 Numerical results

In the following, we present the numerical results obtained for the different experiments described above. Further results beyond those presented here can be found in the accompanying code package [69].

5.2.1 Training overview

The detailed training behavior for selected policies is shown in Figure 5. Since a significant amount of hyperparameter setups did not result in stabilizing policies in the test simulation, in particular for the classical direct DDPG approach, we filtered the results to show in Figure 5 only the five best policies that stabilize the systems with smallest distance to the desired steady state. The training time of UMPO-MA is not included in the plots of MF-UMPO in these figures. Additionally, the training runs of direct DDPG have been restricted in terms of computation time to be at most as long as the overall slowest runs of UMPO for the respective neural network sizes. Comparing the results for the Allen-Cahn equation shows that in both cases the new approaches reach faster higher rewards than direct DDPG. For smaller networks such as (20, 10), the rewards of UMPO behave similar to direct DDPG. UMPO-MA and MF-UMPO provide higher rewards faster during their training phase, but direct DDPG is able to catch up to these after 0.05 h. In contrast, for larger networks such as (400, 200), the new approaches UMPO, UMPO-MA and MF-UMPO clearly outperform the classical direct DDPG method in terms of reward versus training time. While as in Figure 5a it would be possible for direct DDPG to improve its rewards for longer training times, it already runs twice as long as the other approaches implying that significantly more resources are needed for direct DDPG to give higher rewards here. For the tubular reactor, the results in Figures 5c and 5d look very similar to each other, with the rewards of UMPO behaving similar to direct DDPG but with shorter training times. UMPO-MA gives higher rewards than UMPO-MA and UMPO, which are further improved by MF-UMPO. Lastly, we have the Toda lattice example in Figures 5e and 5g as well as in Figures 5f and 5h. The strong nonlinearity is a challenge for reinforcement learning methods that are trained based on querying the high-dimensional system (1). This can be also seen here as direct DDPG, UMPO and MF-UMPO provide similar reward behaviors, while UMPO-MA has the best performance. However, we can see in Figures 5g and 5h that MF-UMPO still yields consistently better rewards than direct DDPG. For this example, UMPO and MF-UMPO achieve improvements by a factor of 2 in terms of the mean rewards over direct DDPG.

In Figure 6, the mean amount of system queries up to the training times 0.02 h for

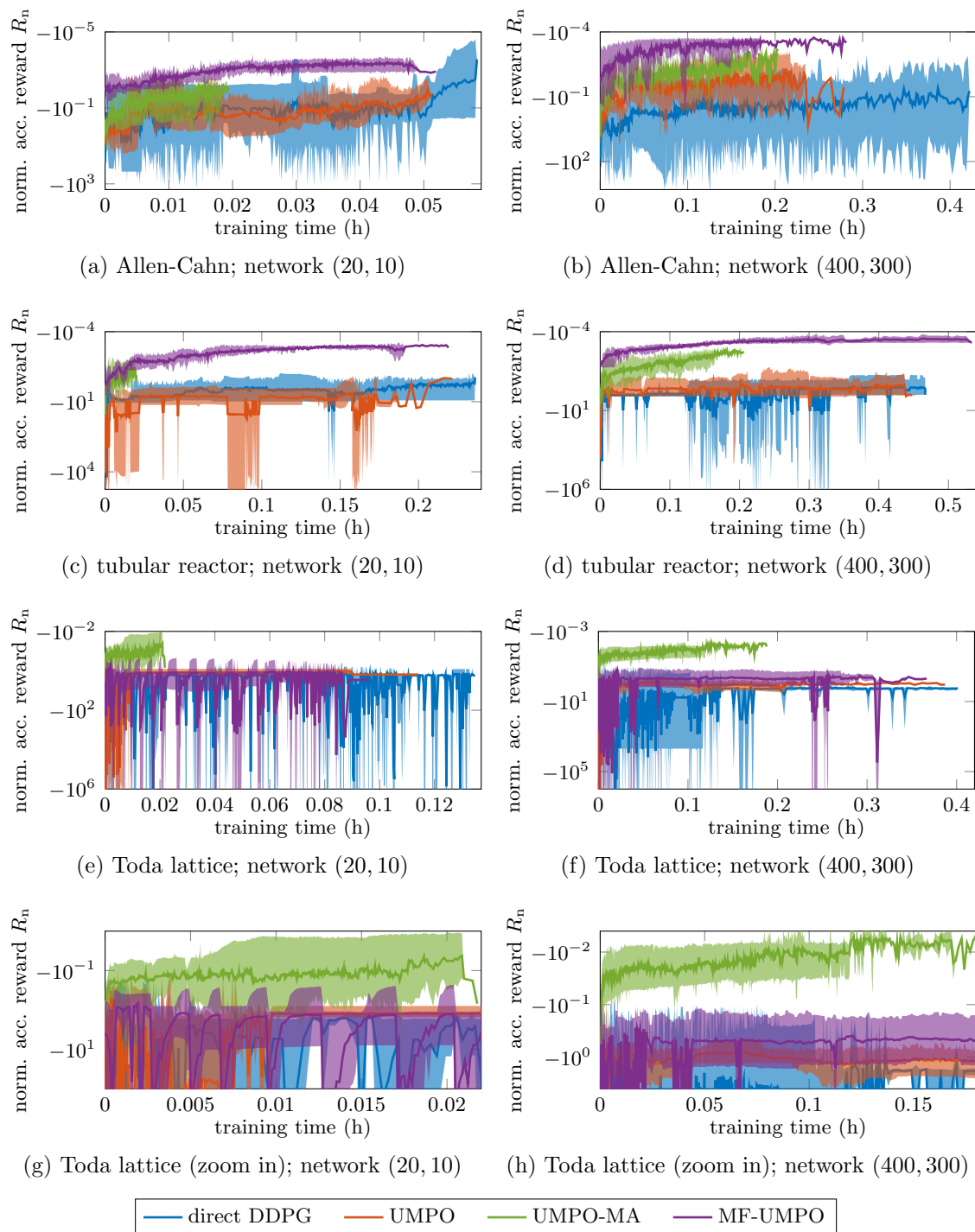


Figure 5: Comparison of normalized accumulated rewards: Plots (a)–(d) show that the approach MF-UMPO that uses the high-dimensional system and the latent model together achieves higher rewards than UMPO-MA that uses the latent model alone. For the Toda lattice example with results shown in (e)–(g), MF-UMPO achieves similar rewards as direct DDPG. Note that in the Toda lattice example, UMPO-MA achieves the highest rewards as the latent model of the unstable dynamics hides many of the strongly nonlinear dynamics that affect the stabilization.

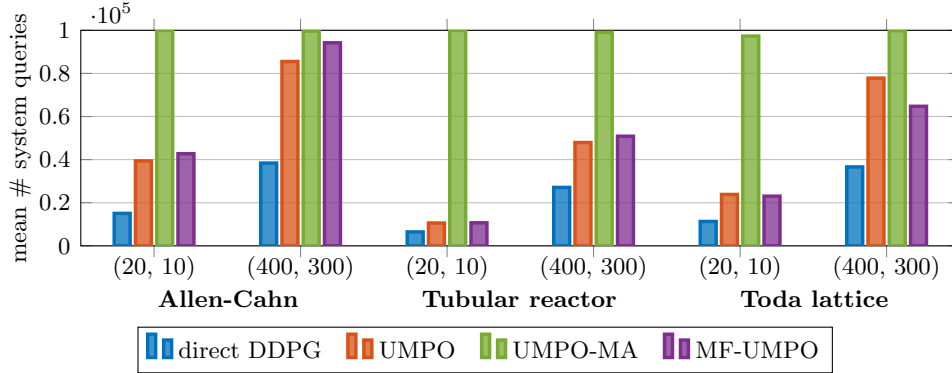


Figure 6: Comparison of the mean amount of system queries after 0.02 h and 0.2 h training time for small and large neural networks. In all examples, UMPO-MA manages to query the latent model at least 10^5 times, which is the maximal amount allowed. UMPO and MF-UMPO manage to query the system more often than direct DDPG, leading to speedups ranging from around 1.7 up to 2.2.

small neural networks and 0.2 h for large neural networks are shown. In all examples, UMPO-MA is able to (nearly) perform the maximum allowed 10^5 system queries. Also, UMPO and MF-UMPO always outperform direct DDPG, with a speed up factor of around 1.7 to 2.2, which allows these methods to reach higher rewards quicker as they can perform more training steps in a smaller amount of time.

5.2.2 Quality of learned policies

To illustrate the results of applying the learned policies, we consider the tubular reactor example and the best performing policies for the neural network size (400, 300) for the policy after 0.2 h of training time. In the following experiments, the initial condition is set to the steady state, $x(0) = \bar{x}$ and a random disturbance is applied up to the physical time $\tau \cdot t = 0.3$ to trigger the system instabilities. We plot the temperature profiles over time in Figure 7. A stabilized system leads to a smooth temperature transition over the space-time domain. The states are strongly oscillating for direct DDPG, while the proposed methods based on the unstable manifolds provide smooth, stabilized simulations. To clearer see the oscillations, we plot the temperature and concentration at the left end of the tube over time in Figure 8. The policy learned by direct DDPG steers the outputs away from the uncontrolled oscillations but is clearly not stabilizing towards the considered steady state, as the concentration deviates far from the initial condition and the temperature is strongly oscillating. In contrast, the policies obtained by the newly proposed methods are stabilizing the system. We can see minor deviations from the steady state in Figure 8b, which become smaller moving to Figure 8c and finally disappear in Figure 8d. The most stable results are given by MF-UMPO, with an at least three orders of magnitude smaller deviation from the desired state when compared to direct DDPG.

5.2.3 Quantitative comparison

The plots in Figure 9 show the training time per learning step and the maximum reward at the end of the learning for the Allen-Cahn, the tubular reactor, and Toda lattice example, respectively. The shown results are averages over the five policies of each network size that stabilize the system closest to the steady state. As can be seen in the top plot of Figure 9, all new approaches show an improvement in terms of their training time per step

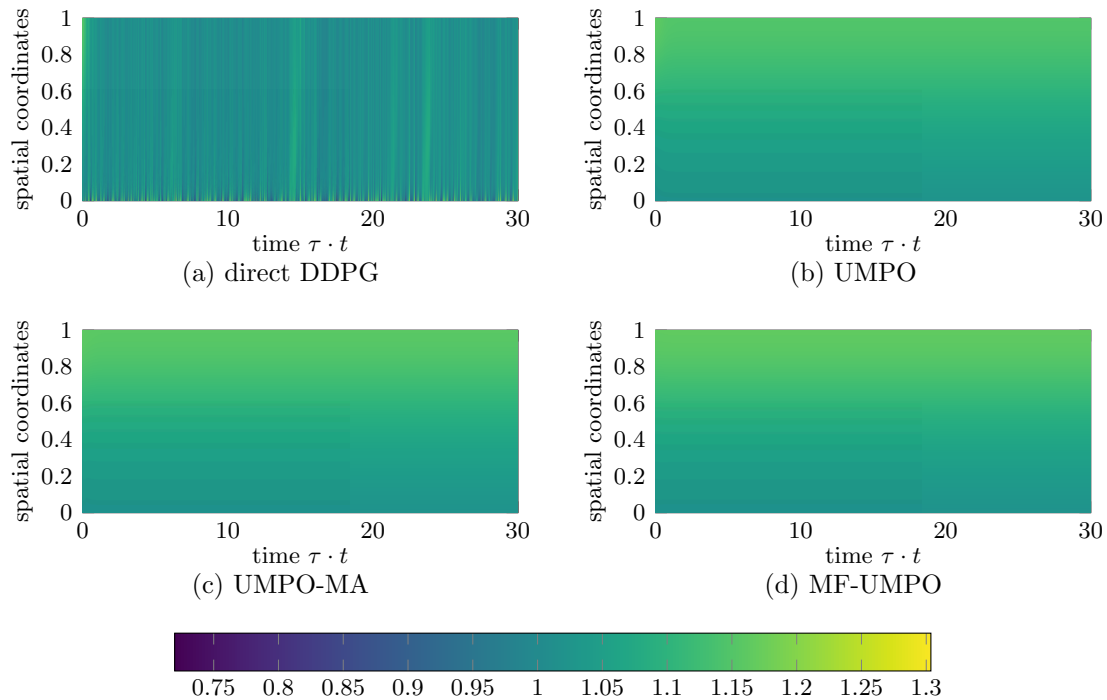


Figure 7: Temperature profiles of the tubular reactor with policies obtained after 0.2 h of training time with neural network architecture (400, 300). The plots show that direct DDPG fails to stabilize the reactor whereas UMPO provides a stabilizing policy, with MF-UMPO achieving lowest oscillations and deriving the system closest to the desired steady state.

compared to the classical direct DDPG method. The time shown for MF-UMPO contains the training of the initial phase with UMPO-MA, but it is still faster for both neural network sizes compared to direct DDPG. The bottom plot shows the best mean rewards that have been reached after 0.02 h of training time using (20, 10) networks and after 0.2 h for the (400, 300) networks. For the smaller networks in the Allen-Cahn and tubular reactor examples, UMPO does not surpass direct DDPG but yields similar rewards. UMPO might improve for longer training times; however, since UMPO provides faster training steps, the smaller neural networks may still be preferred here despite the somewhat lower rewards. UMPO-MA and MF-UMPO are surpassing UMPO and direct DDPG in the Allen-Cahn and tubular reactor examples by at least one and up to two orders of magnitude. The behavior of the methods changes in the Toda lattice example. UMPO-MA provides here the best rewards, which MF-UMPO is not able to preserve or to improve on despite using UMPO-MA as initialization. A possible explanation for these results comes from the strength of the nonlinearity in the example. Even small disturbances can have a catastrophic effect on the states of the system leading to blowups after only few time steps. Such disturbances are difficult to avoid in the training phase of reinforcement learning via stochastic optimization methods, which means that large portions of the data obtained from the nonlinear system for training the learning agents are in unstable regimes already and thus unsuited for training. However, we can see that for the (20, 10) networks, UMPO yields higher rewards than direct DDPG and, for (400, 300), MF-UMPO gives higher rewards than direct DDPG.

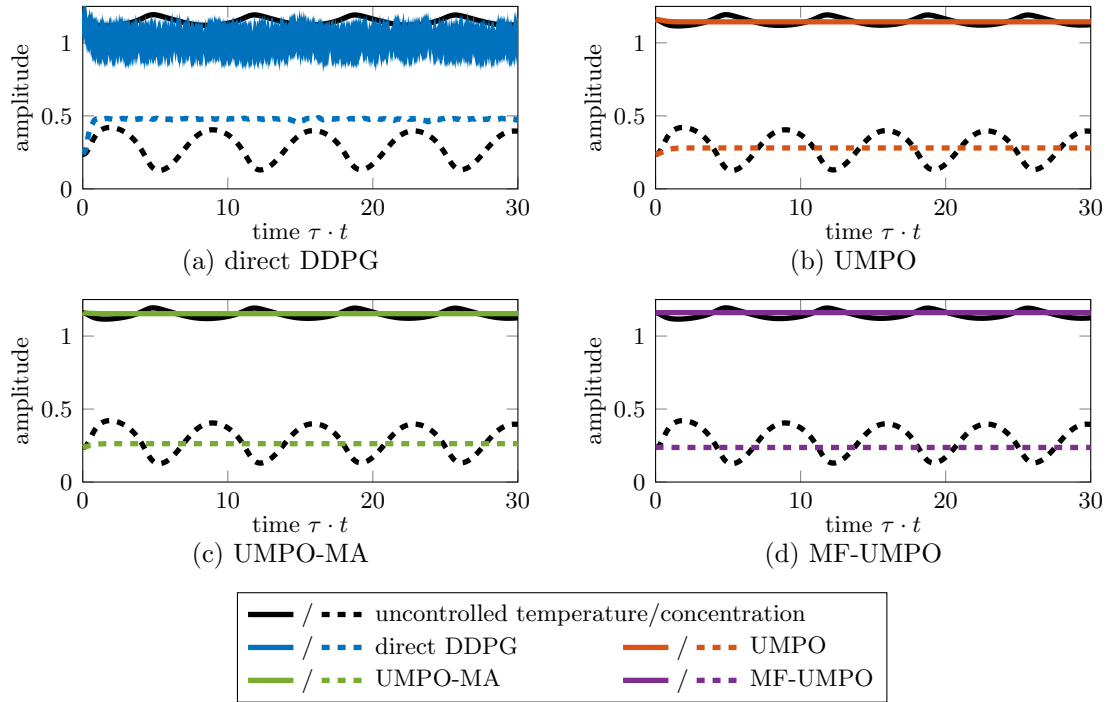


Figure 8: The plots show the outputs of the simulations of the tubular reactor with a policy that is obtained after 0.2 h of training time with neural network architecture (400, 300). The direct DDPG approach fails to stabilize the system within the short training time of 0.2 h because neither temperature nor concentration measurements are close to the steady state. Additionally, the temperature strongly oscillates. The other approaches learn a stabilizing policy within the training time of 0.2 h. Notice that deviations from the steady state decrease in the order of UMPO, UMPO-MA and MF-UMPO; thus the multi-fidelity approach MF-UMPO achieves a stabilization closest to the desired steady state.

5.2.4 Dependence of performance on the state dimension

Figure 10 shows a comparison of the training times for the two neural network sizes (20, 10) and (400, 300) when applied to finer and finer spatial discretizations of the tubular reactor model, which directly corresponds to the state dimension N of the system that is to be stabilized. For both neural network sizes, we can observe the performance improvement of the new methods compared to direct DDPG. For the smaller networks, the training time is clearly dominated by the evaluation time of the high-dimensional system (1) rather than the optimization of the neural networks such that UMPO and MF-UMPO give only an improvement of about 20 – 25% compared to direct DDPG. This factor increases to around 70 – 75% for larger neural networks, which indicates that the proposed methods have increasing benefit as the network sizes grow. The training times for UMPO-MA do not depend on the full state dimension N but on the number of unstable system modes $n = 2$, which is constant even as discretizations are refined. Therefore, these training times are constant up to measurement fluctuations in Figure 10. The training times of UMPO-MA mildly increase for the larger neural networks due to the increase in parameters to learn, which is still negligible small compared to direct DDPG, where the number of parameters in the neural network parametrization scales with the state dimension N . This demonstrates the power of the unstable manifold with a dimension that is fixed even if

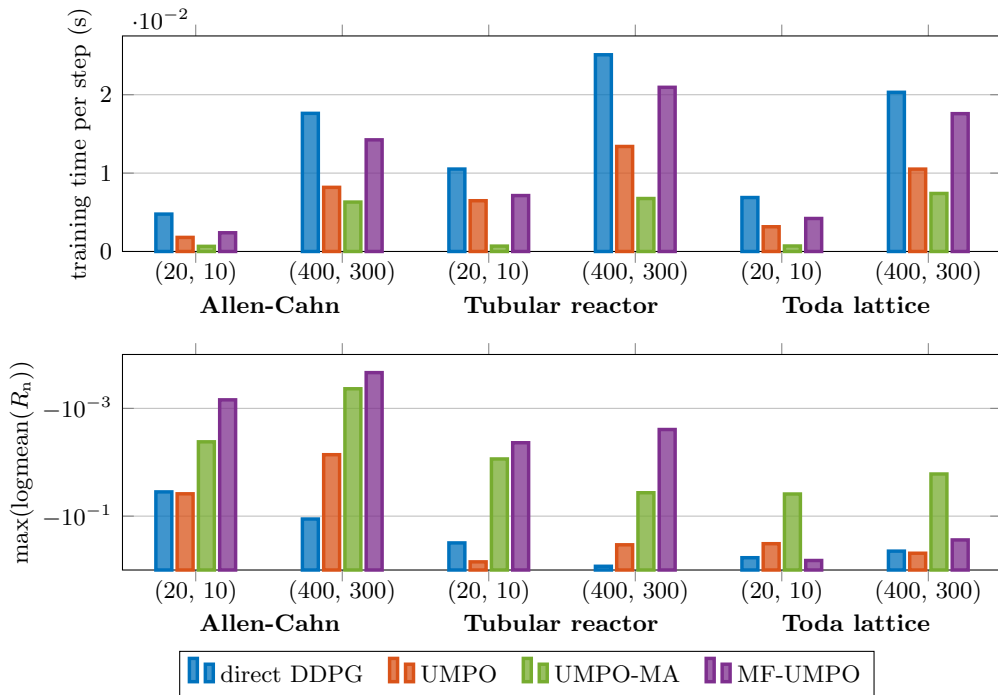


Figure 9: Top shows comparison of the mean training times per step. For all examples, UMPO-MA has the lowest training time per step that is similar across all examples for the same neural network sizes. The method UMPO has the next larger training time per step, followed by MF-UMPO. All new approaches require shorter training times than the classical direct DDPG method. Bottom shows comparison of the best logarithmic means of normalized accumulated rewards after 0.02 h and 0.2 h of training time for small and large neural networks: In all examples, the UMPO-MA initialization achieves up to two orders of magnitude better rewards than direct DDPG. MF-UMPO further improves these rewards with the exception of the Toda lattice model, which contains a challenging non-linear term, which affects the performance of the MF-UMPO policy and due to which the dynamics blow up after only few time steps in the presence of instabilities.

the solution fields of the underlying governing equations are ever finer resolved and thus the state dimension N of the dynamical system (1) grows.

6 Conclusions

In this work, we showed that the latent manifold of unstable dynamics is well suited for finding stabilizing policies with reinforcement learning. The unstable latent manifold can be leveraged either directly with high-dimensional systems or with a two-step, multi-fidelity approach that first trains on latent models and then fine-tunes and ultimately certifies the learned policies on the high-dimensional systems. The proposed approaches based on the unstable latent manifold achieve rewards that are several orders of magnitude higher than the rewards achieved with classical approaches without the unstable latent manifold within a given fixed training time.

While the new methods have been shown to work well in the presented numerical ex-

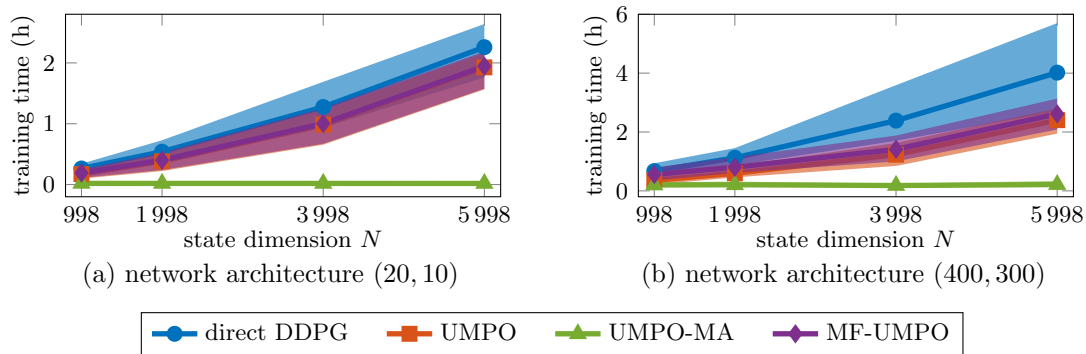


Figure 10: The training times of the direct DDPG, UMPO, UMPO-MA, MF-UMPO approaches are compared for different state-space dimensions of the tubular reactor example. The speedup obtained is about 20–25% for the small networks and 70 – 75% for the large networks. Notice that the training time of UMPO-MA is independent of N and therefore is constant in the shown plots.

amples, there are limitations to them. We considered a small number of unstable system modes, which allowed to consider low-dimensional parametrizations of the policy. This is not the case in all practical applications. In particular for chaotic systems, where the dimension of the unstable manifold scales with $\mathcal{O}(N)$, the new approach is not expected to yield performance improvements.

Acknowledgments

The authors were supported by the Air Force Office of Scientific Research (AFOSR) award FA9550-21-1-0222 (Dr. Fariba Fahroo) and the second author was additionally supported by the National Science Foundation under Grant No. 2012250 and No. 2046521. Parts of this work were carried out while the first author was with the Courant Institute of Mathematical Sciences, New York University, USA.

References

- [1] M. Abadi, P. Barham, J. Chen, Z. Chen, A. Davis, J. Dean, M. Devin, S. Ghemawat, G. Irving, M. Isard, M. Kudlur, J. Levenberg, R. Monga, S. Moore, D. G. Murray, B. Steiner, P. Tucker, V. Vasudevan, P. Warden, M. Wicke, Y. Yu, and X. Zheng. TensorFlow: A system for large-scale machine learning. In *Proceedings of the 12th USENIX Conference on Operating Systems Design and Implementation (OSDI'16)*, pages 265–283, 2016.
- [2] S. M. Allen and J. W. Cahn. Coherent and incoherent equilibria in iron-rich iron-aluminum alloys. *Acta Metall.*, 23(9):1017–1026, 1975. doi:10.1016/0001-6160(75)90106-6.
- [3] A. C. Antoulas, I. V. Gosea, and A. C. Ionita. Model reduction of bilinear systems in the Loewner framework. *SIAM J. Sci. Comput.*, 38(5):B889–B916, 2016. doi:10.1137/15M1041432.
- [4] W. E. Arnoldi. The principle of minimized iterations in the solution of the matrix eigenvalue problem. *Quart. Appl. Math.*, 9:17–29, 1951. doi:10.1090/qam/42792.

- [5] P. Baldi. Autoencoders, unsupervised learning, and deep architectures. *Proceedings of ICML Workshop on Unsupervised and Transfer Learning*, PMLR, 27:37–49, 2012. URL: <https://proceedings.mlr.press/v27/baldi12a.html>.
- [6] J. Barnett and C. Farhat. Quadratic approximation manifold for mitigating the Kolmogorov barrier in nonlinear projection-based model order reduction. *J. Comput. Phys.*, 464:111348, 2022. doi:10.1016/j.jcp.2022.111348.
- [7] P. Benner, S. Gugercin, and K. Willcox. A survey of projection-based model reduction methods for parametric dynamical systems. *SIAM Rev.*, 57(4):483–531, 2015. doi:10.1137/130932715.
- [8] P. Benner, J. Heiland, and S. W. R. Werner. Robust output-feedback stabilization for incompressible flows using low-dimensional \mathcal{H}_∞ -controllers. *Comput. Optim. Appl.*, 82(1):225–249, 2022. doi:10.1007/s10589-022-00359-x.
- [9] J. Berman and B. Peherstorfer. CoLoRA: Continuous low-rank adaptation for reduced implicit neural modeling of parameterized partial differential equations. e-print 2402.14646, arXiv, 2024. Machine Learning (cs.LG). doi:10.48550/arXiv.2402.14646.
- [10] J. Bradbury, R. Frostig, P. Hawkins, M. J. Johnson, C. Leary, D. Maclaurin, G. Necula, A. Paszke, J. VanderPlas, S. Wanderman-Milne, and Q. Zhang. JAX: composable transformations of Python+NumPy programs (version 0.3.13), May 2022. URL: <https://github.com/google/jax>.
- [11] H. Broer and F. Takens. *Dynamical Systems and Chaos*, volume 172 of *Applied Mathematical Sciences*. Springer, New York, NY, 2011. doi:10.1007/978-1-4419-6870-8.
- [12] S. L. Brunton, B. W. Brunton, J. L. Proctor, and J. N. Kutz. Koopman invariant subspaces and finite linear representations of nonlinear dynamical systems for control. *PLoS ONE*, 11(2):e0150171, 2016. doi:10.1371/journal.pone.0150171.
- [13] S. L. Brunton and J. N. Kutz. *Data-Driven Science and Engineering: Machine Learning, Dynamical Systems, and Control*. Cambridge University Press, Cambridge, 2019. doi:10.1017/9781108380690.
- [14] S. L. Brunton, J. L. Proctor, and J. N. Kutz. Discovering governing equations from data by sparse identification of nonlinear dynamical systems. *Proc. Natl. Acad. Sci. U. S. A.*, 113(15):3932–3937, 2016. doi:10.1073/pnas.1517384113.
- [15] N. Chafee and E. N. Infante. A bifurcation problem for a nonlinear partial differential equation of parabolic type. *Appl. Anal.*, 4(1):17–37, 2007. doi:10.1080/00036817408839081.
- [16] Z. Drmač and B. Peherstorfer. Learning low-dimensional dynamical-system models from noisy frequency-response data with Loewner rational interpolation. In C. Beattie, P. Benner, M. Embree, S. Gugercin, and S. Lefteriu, editors, *Realization and Model Reduction of Dynamical Systems*, pages 39–57. Springer, Cham, 2022. doi:10.1007/978-3-030-95157-3_3.
- [17] M. Fliess and C. Join. Model-free control. *Int. J. Control*, 86(12):2228–2252, 2013. doi:10.1080/00207179.2013.810345.

- [18] S. Fujimoto, H. Van Hoof, and D. Meger. Addressing function approximation error in actor-critic methods. *Proceedings of the 35th International Conference on Machine Learning, PMLR*, 80:1587–1596, 2018. URL: <https://proceedings.mlr.press/v80/fujimoto18a.html>.
- [19] R. Geelen, S. Wright, and K. Willcox. Operator inference for non-intrusive model reduction with quadratic manifolds. *Comput. Methods Appl. Mech. Eng.*, 403, Part B:115717, 2023. doi:10.1016/j.cma.2022.115717.
- [20] O. Ghattas and K. Willcox. Learning physics-based models from data: perspectives from inverse problems and model reduction. *Acta Numer.*, 30:445–554, 2021. doi:10.1017/S0962492921000064.
- [21] G. H. Golub and C. F. Van Loan. *Matrix Computations*. Johns Hopkins Studies in the Mathematical Sciences. Johns Hopkins University Press, Baltimore, fourth edition, 2013.
- [22] D. Görge. Distributed adaptive linear quadratic control using distributed reinforcement learning. *IFAC-Pap.*, 52(11):218–223, 2019. 5th IFAC Conference on Intelligent Control and Automation Sciences ICONS 2019. doi:10.1016/j.ifacol.2019.09.144.
- [23] I. V. Gosea and A. C. Antoulas. Data-driven model order reduction of quadratic-bilinear systems. *Numer. Linear Algebra Appl.*, 25(6):e2200, 2018. doi:10.1002/nla.2200.
- [24] B. Gravell, P. M. Esfahani, and T. Summers. Learning optimal controllers for linear systems with multiplicative noise via policy gradient. *IEEE Trans. Autom. Control*, 66(11):5283–5298, 2021. doi:10.1109/TAC.2020.3037046.
- [25] R. F. Heinemann and A. B. Poore. Multiplicity, stability, and oscillatory dynamics of the tubular reactor. *Chem. Eng. Sci.*, 36(9):1411–1419, 1981. doi:10.1016/0009-2509(81)80175-3.
- [26] T. Kadeethum, F. Ballarin, Y. Choi, and D. and O’Malley. Non-intrusive reduced order modeling of natural convection in porous media using convolutional autoencoders: Comparison with linear subspace techniques. *Adv. Water Resour.*, 160:104098, 2022. doi:10.1016/j.advwatres.2021.104098.
- [27] T. Kadeethum, D. O’Malley, J. N. Fuhg, Y. Choi, J. Lee, H. S. Viswanathan, and N. Bouklas. A framework for data-driven solution and parameter estimation of PDEs using conditional generative adversarial networks. *Nat. Comput. Sci.*, 1(12):819–829, 2021. doi:10.1038/s43588-021-00171-3.
- [28] D. C. Karnopp, D. L. Margolis, and R. C. Rosenberg. *System Dynamics: Modeling, Simulation, and Control of Mechatronic Systems*. Wiley, Hoboken, NJ, fifth edition, 2012. doi:10.1002/9781118152812.
- [29] Y. Kim, Y. Choi, D. Widemann, and T. Zohdi. A fast and accurate physics-informed neural network reduced order model with shallow masked autoencoder. *J. Comput. Phys.*, 451:110841, 2022. doi:10.1016/j.jcp.2021.110841.
- [30] I. Kostrikov. JAXRL: Implementations of reinforcement learning algorithms in JAX (version 0.0.7), September 2022. Version commit SHA: bc8030c. URL: <https://github.com/ikostrikov/jaxrl>.

- [31] B. Kramer, B. Peherstorfer, and K. E. Willcox. Learning nonlinear reduced models from data with operator inference. *Annu. Rev. Fluid Mech.*, 56:521–548, 2024. doi:[10.1146/annurev-fluid-121021-025220](https://doi.org/10.1146/annurev-fluid-121021-025220).
- [32] B. Kramer and K. E. Willcox. Nonlinear model order reduction via lifting transformations and proper orthogonal decomposition. *AIAA J.*, 57(6):2297–2307, 2019. doi:[10.2514/1.J057791](https://doi.org/10.2514/1.J057791).
- [33] M. A. Kramer. Nonlinear principal component analysis using autoassociative neural networks. *AIChE J.*, 37(2):233–243, 1991. doi:[10.1002/aic.690370209](https://doi.org/10.1002/aic.690370209).
- [34] B. Krauskopf, H. M. Osinga, E. J. Doedel, M. E. Henderson, J. Guckenheimer, A. Vladimirov, M. Dellnitz, and O. Junge. A survey of methods for computing (un)stable manifolds of vector fields. *Int. J. Bifurc. Chaos Appl. Sci. Eng.*, 15(3):763–791, 2005. doi:[10.1142/S0218127405012533](https://doi.org/10.1142/S0218127405012533).
- [35] J. N. Kutz, S. L. Brunton, B. W. Brunton, and J. L. Proctor. *Dynamic Mode Decomposition: Data-Driven Modeling of Complex Systems*. SIAM, Philadelphia, PA, 2016. doi:[10.1137/1.9781611974508](https://doi.org/10.1137/1.9781611974508).
- [36] Y. Li, Y. Tang, R. Zhang, and N. Li. Distributed reinforcement learning for decentralized linear quadratic control: A derivative-free policy optimization approach. *IEEE Trans. Autom. Control*, 67(12):6429–6444, 2022. doi:[10.1109/TAC.2021.3128592](https://doi.org/10.1109/TAC.2021.3128592).
- [37] T. P. Lillicrap, J. J. Hunt, A. Pritzel, N. Heess, T. Erez, Y. Tassa, D. Silver, and D. Wierstra. Continuous control with deep reinforcement learning. e-print 1509.02971, arXiv, 2015. Machine Learning (cs.LG). doi:[10.48550/arXiv.1509.02971](https://doi.org/10.48550/arXiv.1509.02971).
- [38] A. Locatelli. *Optimal Control: An Introduction*. Birkhäuser, Basel, 2001.
- [39] D. Malik, A. Pananjady, K. Bhatia, K. Khamaru, P. Bartlett, and M. Wainwright. Derivative-free methods for policy optimization: Guarantees for linear quadratic systems. In K. Chaudhuri and M. Sugiyama, editors, *Proceedings of the Twenty-Second International Conference on Artificial Intelligence and Statistics*, PMLR, pages 2916–2925, 2019. URL: <https://proceedings.mlr.press/v89/malik19a.html>.
- [40] A. J. Mayo and A. C. Antoulas. A framework for the solution of the generalized realization problem. *Linear Algebra Appl.*, 425(2–3):634–662, 2007. Special issue in honor of P. A. Fuhrmann, Edited by A. C. Antoulas, U. Helmke, J. Rosenthal, V. Vinnikov, and E. Zerz. doi:[10.1016/j.laa.2007.03.008](https://doi.org/10.1016/j.laa.2007.03.008).
- [41] I. Mezić. Spectral properties of dynamical systems, model reduction and decompositions. *Nonlinear Dyn.*, 41(1–3):309–325, 2005. doi:[10.1007/s11071-005-2824-x](https://doi.org/10.1007/s11071-005-2824-x).
- [42] S. K. Mitusch, S. W. Funke, and J. S. Dokken. dolfin-adjoint 2018.1: automated adjoints for FEniCS and Firedrake. *J. Open Source Softw.*, 4(38):1292, 2019. doi:[10.21105/joss.01292](https://doi.org/10.21105/joss.01292).
- [43] H. Mohammadi, A. Zare, M. Soltanolkotabi, and M. R. Jovanović. Convergence and sample complexity of gradient methods for the model-free linear–quadratic regulator problem. *IEEE Trans. Autom. Control*, 67(5):2435–2450, 2022. doi:[10.1109/TAC.2021.3087455](https://doi.org/10.1109/TAC.2021.3087455).

- [44] B. C. Moore. Principal component analysis in linear systems: controllability, observability, and model reduction. *IEEE Trans. Autom. Control*, AC-26(1):17–32, 1981. doi:10.1109/TAC.1981.1102568.
- [45] D. Mustafa and K. Glover. Controller reduction by \mathcal{H}_∞ -balanced truncation. *IEEE Trans. Autom. Control*, 36(6):668–682, 1991. doi:10.1109/9.86941.
- [46] H. Nijmeijer and A. Van der Schaft. *Nonlinear Dynamical Control Systems*. Springer, New York, NY, fourth edition, 2016. doi:10.1007/978-1-4757-2101-0.
- [47] A. Paszke, S. Gross, F. Massa, A. Lerer, J. Bradbury, G. Chanan, T. Killeen, Z. Lin, N. Gimeshein, L. Antiga, A. Desmaison, A. Kopf, E. Yang, Z. DeVito, M. Raison, A. Tejani, S. Chilamkurthy, B. Steiner, L. Fang, J. Bai, and S. Chintala. PyTorch: An imperative style, high-performance deep learning library. In H. Wallach, H. Larochelle, A. Beygelzimer, F. d’Alché Buc, E. Fox, and R. Garnett, editors, *Advances in Neural Information Processing Systems*, volume 32, pages 8026–8037, 2019.
- [48] K. Pearson. On lines and planes of closest fit to systems of points in space. *Philos. Mag.*, 2(11):559–572, 1901. doi:10.1080/14786440109462720.
- [49] B. Peherstorfer. Sampling low-dimensional Markovian dynamics for preasymptotically recovering reduced models from data with operator inference. *SIAM J. Sci. Comput.*, 42(5):A3489–A3515, 2020. doi:10.1137/19M1292448.
- [50] B. Peherstorfer and K. Willcox. Data-driven operator inference for nonintrusive projection-based model reduction. *Comput. Methods Appl. Mech. Eng.*, 306:196–215, 2016. doi:10.1016/j.cma.2016.03.025.
- [51] B. Peherstorfer, K. Willcox, and M. Gunzburger. Survey of multifidelity methods in uncertainty propagation, inference, and optimization. *SIAM Rev.*, 60(3):550–591, 2018. doi:10.1137/16M1082469.
- [52] E. Qian, B. Kramer, B. Peherstorfer, and K. Willcox. Lift & Learn: Physics-informed machine learning for large-scale nonlinear dynamical systems. *Phys. D: Nonlinear Phenom.*, 406:132401, 2020. doi:10.1016/j.physd.2020.132401.
- [53] B. Recht. A tour of reinforcement learning: The view from continuous control. *Annu. Rev. Control Robot. Auton. Syst.*, 2:253–279, 2019. doi:10.1146/annurev-control-053018-023825.
- [54] C. W. Rowley, I. Mezić, S. Bagheri, P. Schlatter, and D. S. Henningson. Spectral analysis of nonlinear flows. *J. Fluid Mech.*, 641:115–127, 2009. doi:10.1017/S0022112009992059.
- [55] N. Sawant, B. Kramer, and B. Peherstorfer. Physics-informed regularization and structure preservation for learning stable reduced models from data with operator inference. *Comput. Methods Appl. Mech. Eng.*, 404:115836, 2023. doi:10.1016/j.cma.2022.115836.
- [56] H. Schaeffer, G. Tran, and R. Ward. Extracting sparse high-dimensional dynamics from limited data. *SIAM J. Appl. Math.*, 78(6):3279–3295, 2018. doi:10.1137/18M116798X.

- [57] P. J. Schmid. Dynamic mode decomposition of numerical and experimental data. *J. Fluid Mech.*, 656:5–28, 2010. doi:10.1017/S0022112010001217.
- [58] P. Schulze and B. Unger. Data-driven interpolation of dynamical systems with delay. *Syst. Control Lett.*, 97:125–131, 2016. doi:10.1016/j.sysconle.2016.09.007.
- [59] P. Schulze, B. Unger, C. Beattie, and S. Gugercin. Data-driven structured realization. *Linear Algebra Appl.*, 537:250–286, 2018. doi:10.1016/j.laa.2017.09.030.
- [60] P. Schwerdtner and B. Peherstorfer. Greedy construction of quadratic manifolds for nonlinear dimensionality reduction and nonlinear model reduction. e-print 2403.06732, arXiv, 2024. Numerical Analysis (math.NA). doi:10.48550/arXiv.2403.06732.
- [61] H. Sharma, Z. Wang, and B. Kramer. Hamiltonian operator inference: Physics-preserving learning of reduced-order models for canonical Hamiltonian systems. *Phys. D: Nonlinear Phenom.*, 431:133122, 2022. doi:10.1016/j.physd.2021.133122.
- [62] E. Silverman. *Methodological Investigations in Agent-Based Modelling: With Applications for the Social Sciences*, volume 13 of *Methodos Series*. Springer, Cham, 2018. doi:10.1007/978-3-319-72408-9.
- [63] G. W. Stewart. A Krylov–Schur algorithm for large eigenproblems. *SIAM J. Matrix Anal. Appl.*, 23(3):601–614, 2001. doi:10.1137/S0895479800371529.
- [64] R. S. Sutton and A. G. Barto. *Reinforcement Learning: An Introduction*. MIT Press, Cambridge, MA, second edition, 2018. URL: <http://incompleteideas.net/book/the-book-2nd.html>.
- [65] M. Toda. Vibration of a chain with nonlinear interaction. *J. Phys. Soc. Jpn.*, 22(2):431–436, 1967. doi:10.1143/JPSJ.22.431.
- [66] J. H. Tu, C. W. Rowley, D. M. Luchtenburg, S. L. Brunton, and J. N. Kutz. On dynamic mode decomposition: Theory and applications. *J. Comput. Dyn.*, 1(2):391–421, 2014. doi:10.3934/jcd.2014.1.391.
- [67] P. R. Vlachas, G. Arampatzis, C. Uhler, and P. Koumoutsakos. Multiscale simulations of complex systems by learning their effective dynamics. *Nat. Mach. Intell.*, 4(4):359–366, 2022. doi:10.1038/s42256-022-00464-w.
- [68] S. W. R. Werner. *Structure-Preserving Model Reduction for Mechanical Systems*. Dissertation, Otto-von-Guericke-Universität, Magdeburg, Germany, 2021. doi:10.25673/38617.
- [69] S. W. R. Werner. Code, data and results for numerical experiments in “System stabilization with policy optimization on unstable latent manifolds” (version 1.0), April 2024. doi:10.5281/zenodo.7897240.
- [70] S. W. R. Werner, M. L. Overton, and B. Peherstorfer. Multifidelity robust controller design with gradient sampling. *SIAM J. Sci. Comput.*, 45(2):A933–A957, 2023. doi:10.1137/22M1500137.
- [71] S. W. R. Werner and B. Peherstorfer. Context-aware controller inference for stabilizing dynamical systems from scarce data. *Proc. R. Soc. A: Math. Phys. Eng. Sci.*, 479(2270):20220506, 2023. doi:10.1098/rspa.2022.0506.

-
- [72] S. W. R. Werner and B. Peherstorfer. On the sample complexity of stabilizing linear dynamical systems from data. *Found. Comput. Math.*, 24(3):955–987, 2024. doi:[10.1007/s10208-023-09605-y](https://doi.org/10.1007/s10208-023-09605-y).
- [73] M. O. Williams, I. G. Kevrekidis, and C. W. Rowley. A data-driven approximation of the Koopman operator: Extending dynamic mode decomposition. *J. Nonlinear Sci.*, 25(6):1307–1346, 2015. doi:[10.1007/s00332-015-9258-5](https://doi.org/10.1007/s00332-015-9258-5).
- [74] J. Ziegler and N. Nichols. Optimum settings for automatic controllers. *Trans. ASME*, 64:759–768, 1942.
- [75] A. Ziessler, M. Dellnitz, and R. Gerlach. The numerical computation of unstable manifolds for infinite dimensional dynamical systems by embedding techniques. *SIAM J. Appl. Dyn. Syst.*, 18(3):1265–1292, 2019. doi:[10.1137/18M1204395](https://doi.org/10.1137/18M1204395).